Transient heat transfer in reciprocating devices – physical model and model validation

Manuel Rexer, Benedict Depp, Peter F. Pelz*

Technische Universität Darmstadt, Chair of Fluidsystems (FST), Otto-Berndt-Straße 2, D-64287 Darmstadt, Germany*
E-Mail: Peter.Pelz@tu-darmstadt.de

In complex fluid systems energy is stored by compressing gas volumes in components, i.e. air springs or hydraulic accumulators. Designing a dynamic fluid system, the behaviour of these devices is strongly influenced by the heat transfer between the gas and the environment. This work aims on extending former investigations regarding heat transfer in the operation of air springs and accumulators. A generalised model for dynamic heat transfer behaviour is derived. Therefore, an equivalent circuit diagram (lumped-element model) for heat flow and driving temperature difference is introduced and parametrised. For the parametrisation the dependency of thermal boundary layer thickness upon excitation frequency is used.

Keywords: dynamic stiffness, heat transfer, linear analogous model, accumulator
Target audience: mobile hydraulics, hydraulic industry, design process

1 Introduction

Hydraulic accumulators, air springs and Stirling engines all serve as energy storing components in complex fluid systems. All devices are based on a common working principle, namely periodic compression and expansion of an enclosed gas. Prominent examples are hydropneumatic suspension systems in mobile applications. In this system, a hydraulic accumulator acts as a spring. Heat transfer between gas and the environment significantly determines the pressure response of this device.

Hence, most of the measures $\phi(t) = \phi(t + 1/f)$ are cyclic with respect to time t and frequency f. Depending on the excitation frequency f the gases change of state is within the isothermal or adiabatic limit [1]. Dynamic simulations of fluid power systems therefore require models capable of describing frequency dependent heat transfer behaviour in reciprocating devices.

The common engineer's approach for modelling heat transfer relies on Newton's law and similarity theory, hence $\dot{Q} \propto Nu\, \lambda\, A\, (T_a - T)$ with heat flow $\dot{Q}$, ambient temperature T_a, average system's temperature T. The Nusselt number Nu is nothing but a dimensionless heat transfer coefficient given as a function of Reynolds number, Prandtl number and Grashof number $Nu = \mathrm{fn}(Re, Pr, Gr)$. The mathematical structure of Newton's law with given Nusselt number implies the phase difference φ between heat flow $\dot{Q}(t)$ and the temperature $T(t)$ to be $\varphi = \angle\left(\dot{Q}(t)/T(t)\right) = \pi$. This holds for $\dot{Q} < 0$ for heat withdrawn from the working gas. However, research shows that in periodically excited gas volumes the transferred amount of heat can be influenced by the formation of thermal boundary layers which also cause φ to shift from π [2]. The mathematical structure of Newton's law is inadequate for describing the accompanying dynamic effect of the boundary layers on heat transfer.

To account for phase shift behaviour Kornhauser [3] has generalised Newton's law by introducing a complex heat flow. Consequently, heat transfer for harmonic excitations with angular frequency $\Omega = 2\pi f$ of gas springs can be modelled using a complex Nusselt number $Nu = Nu' + \mathrm{i}\, Nu''$. All investigations were done using cylindrical test objects. To check the applicability of Kornhauser's modelling approach we determined the response behaviour of commercial hydraulic accumulators of different size and load pressures, cf. Hartig et al. [2]. Figure 1 shows the

frequency-dependent characteristic of the real and imaginary part of the obtained complex Nusselt numbers. Thereupon a lumped parameter model for transfer behaviour of hydraulic accumulators has been derived from the results.

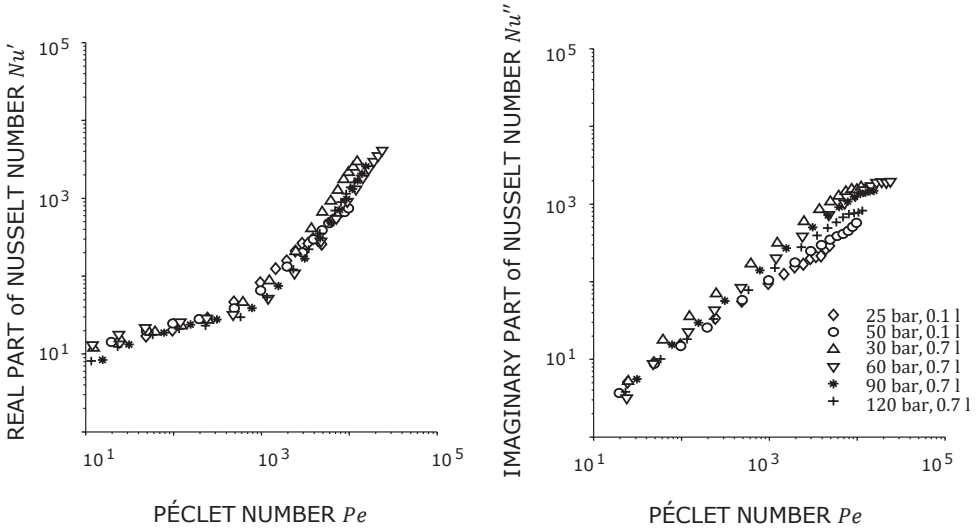

Figure 1: Results of complex Nusselt number $Nu := Nu' + i\,Nu''$ for hydraulic accumulators of different size and load pressures from Hartig et al. [2]

This complex approach is the starting point within the present work for modelling the heat transfer and derive a universally applicable lumped parameter model for the transfer behaviour for pressure and temperature for reciprocating devices. Model parts are the confined gas volume, bounding wall and subsequent environment. The model can be applied in early design phases for optimisation and in controller design. Hence, we further use the analogy to electrical circuits to derive an analogous model whose elements consist of several capacities C_i and resistances R_i to describe heat flow between gas volume and the environment. The structure of the lumped-element circuit model is derived by investigating thermal boundary layer formation using a one-dimensional analytical model by Pelz and Buttenbender [1]. One focus is on the frequency-dependent boundary layer thickness $\delta(\Omega)$.

2 Dynamic lumped parameter model

We consider a zero-dimensional modelling approach for a reciprocating device with a gas as working fluid. The gas is assumed calorically and thermally ideal. We use the conservation equations for the control volume shown in Figure 2. The device is excited by a moving, impermeable piston.

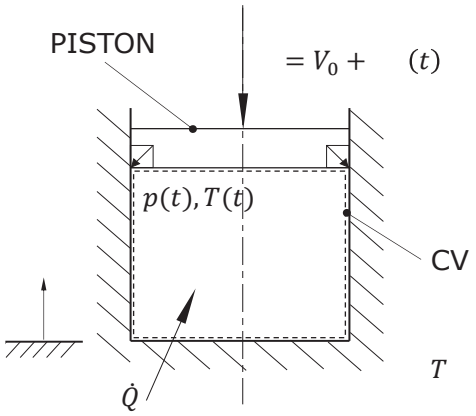

Figure 2: Generic enclosed gas volume with a moving piston; Heat is transferred between the gas and the environment.

A common lumped parameter approach for modelling a system of this kind [1, 4, 5] is given by mass and energy equation, that read

$$\varrho\,\dot{V} + \dot{\varrho}\,V = 0, \tag{1}$$

with time-dependent density $\varrho = \mathrm{fn}(t)$ and volume $V = \mathrm{fn}(t)$ and

$$\dot{} + \gamma\,\dot{p}V = (1-\gamma)\dot{Q}, \tag{2}$$

with isentropic exponent γ and the heat flow between the gas and the environment $\dot{Q}$. The thermal equation of state

$$= \varrho\mathcal{R}T \tag{3}$$

is used as constitutive equation. The working fluid nitrogen exhibits ideal behaviour with only minor deviations to real one up to a pressure of 200 bar at ambient temperature, i.e. compressibility factor $\mathcal{Z}\sim 1$ [6].

The present work's main objective is to quantify the heat flow $\dot{Q}$ or heat flux $\dot{q} \coloneqq \dot{Q}/A$ respectively that is exchanged between gas and environment. In order to do so the thermal boundary layer formation following the work of Pelz and Buttenbender [1] is analysed first. Within this previous work Pelz and Buttenbender [1] derived a generic one-dimensional model for a dynamically excited gas volumes. This model predicts the formation of oscillating boundary layers for density and temperature near the wall for above a certain excitation frequency.

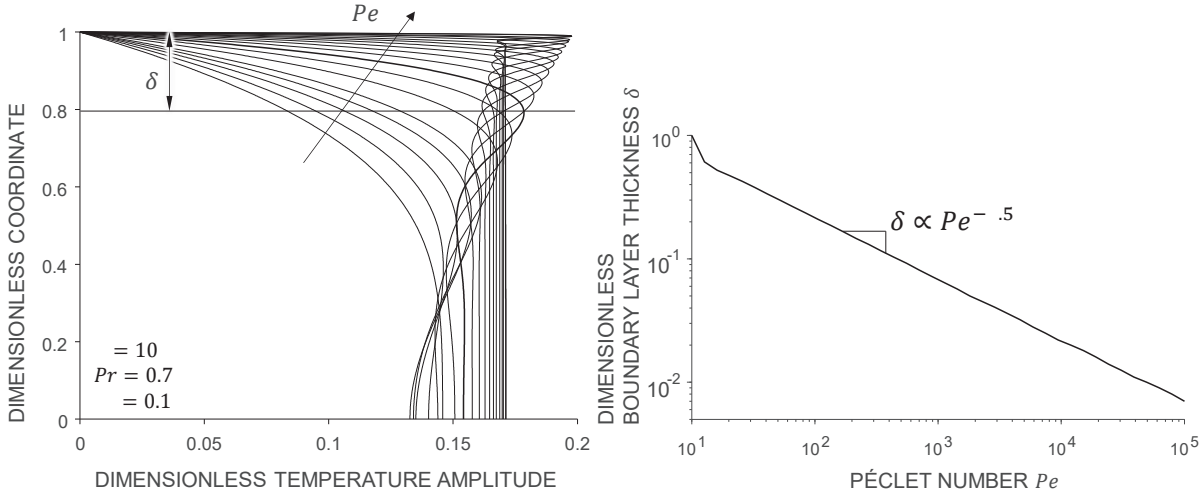

Figure 3: The left plot shows the thermal boundary layer as dimensionless temperature amplitude [1]. The plot on the right side shows the thickness of the boundary layer $\delta = fn(Pe)$. A power law is shown, independent of the other dimensionless quantities.

Analogous to the velocity boundary layer thickness δ of laminar flows along a flat plate whose dependency upon Reynolds number is $\delta \propto Re^{-0.5}$ [7], the thickness of the thermal boundary layer is proportional to the Péclet number $\delta \propto Pe^{-0.5}$. The Péclet number Pe as a dimensionless measure of frequency is defined as

$$Pe \coloneqq \Omega\frac{c_\mathrm{p}\,\varrho}{\lambda\,s^2}, \tag{4}$$

with frequency of excitation f, heat capacity c_p, density ϱ and the thermal conductivity λ of the gas. The reciprocal characteristic length L is given by the volume specific surface area $s \coloneqq A/V$ which equals $s = 6/d$ for a sphere and $s \approx 4/d$ for a cylinder. The characteristic length L of our system is determined independently of geometry by the specific surface area $s = A/V = L^{-1}$ with the surface area A [1].

Simulations show that the pressure is uniformly distributed throughout the volume [1]. This is plausibilised by noting that the Helmholtz number He is much smaller than unity for this problem:

$$He \coloneqq \frac{L\,f}{a} \sim 10^{-2} \ll 1, \tag{5}$$

with the speed of sound $a = \sqrt{\gamma RT}$, the stimulation frequency f and the characteristic length L ($L \sim 10^{-1}$ m, $f \sim 10^{1}$ Hz, $a \sim 10^{2}$ m/s). This implies that the product of temperature and density must also be constant throughout the volume

$$T(t,z)\varrho(t,z) = \text{const.} \tag{6}$$

As temperature is inversely proportional to the density $T \propto \varrho^{-1}$, inertia of the gas molecules leads to an additional thermal capacity in the system, cf. Figure 4.

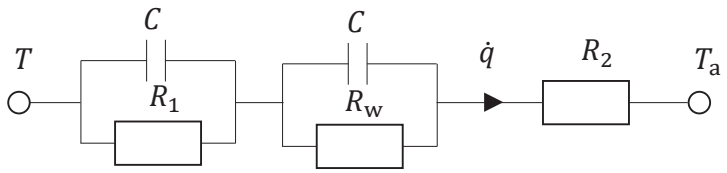

Figure 4: Thermal equivalent circuit diagram of heat transmission between the gas volume with temperature T and the environment with ambient temperature T_a.

The resulting complex heat flux $\dot{q}$ is connected to the driving complex temperature difference $\Delta T = T - T_\mathrm{a}$ via a frequency-dependent impedance $Z(\Omega)$. The resulting resistance law equivalent to an electric circuit reads

$$\dot{q}(t) = \frac{T - T_\mathrm{a}}{Z(\Omega)}. \tag{7}$$

Analysing the network given in Figure 4 the total impedance $Z(\Omega)$ is determined by a series connection of three impedances, i.e. (i) the resistance to heat transfer through the thermal boundary layer at the inner wall. The boundary layer can act as a capacitor C_bound and is connected with a resistance R_1 in parallel. (ii) The thermal impedance of the solid wall consisting of the wall capacity C_wall and resistance R_wall in parallel. (iii) Resistance to heat transfer by natural convection to the surroundings captured by resistance R_2. This leads to a total impedance

$$Z(\Omega) = \frac{R_1}{\mathrm{i}\Omega C \quad + 1} + \frac{R_\mathrm{w}}{\mathrm{i}\Omega C_\mathrm{wall} R_\mathrm{wall} + 1} + R_3. \tag{8}$$

The resistance R_1 is determined with the reported value of a local $Nu' = 3$ by of Pelz and Buttenbender [1], that is obtained by correlating model and measurements for small excitation frequencies

$$R_1 = \lambda\, Nu'\, s^2, \text{ with } Nu' = 3 \text{ [1]}. \tag{9}$$

For the thermal resistance of the solid wall we assume an average wall thickness l_wall and for simplicity only one material with isotropic material properties, i.e. thermal conductivity λ_wall, density ϱ_wall and specific heat capacity c

$$R_\mathrm{wall} = \frac{\lambda_\mathrm{wall}}{l}, \tag{10}$$

$$C_\mathrm{wall} = c_\mathrm{wall}\, \varrho_\mathrm{wall}\, l \quad . \tag{11}$$

The heat transfer resistance between the outer surface and the environment is described by a correlation between Nusselt number Nu, the Grashof number Gr and Prandtl number Pr

$$R_2 = \mathrm{fn}(Nu(Gr, Pr)), \tag{12}$$

where Gr depends on the instantaneous temperature difference between surface temperature and ambient temperature. This has to be calculated iteratively in every time step of the simulation. Since this temperature difference is small, the resistance is also negligibly small $R_2 \to 0$.

From the analysis of the thermal boundary layer, a nonlinear relationship $C = \mathrm{fn}(\Omega)$ could be assumed. However, as a first approximation, we consider a constant capacitance $C = \mathrm{const}$. Since the capacitive effect arises from the spatial mass distribution of the gas, C must be a function of the density and the gas constant $C = \mathrm{fn}(\varrho, \mathcal{R}, s)$. For dimensional reasons, the problem still depends on the specific surface area s, which leads to the relation

$$C \propto \frac{\mathcal{R}\,\varrho}{s}. \tag{13}$$

The arbitrary proportionality constant K can be derived from experimental data. To compare the network model with the previous models [1, 2] we use the Nusselt number as reciprocal impedance

$$Nu := \frac{1}{Z\,\lambda\,s}. \tag{13}$$

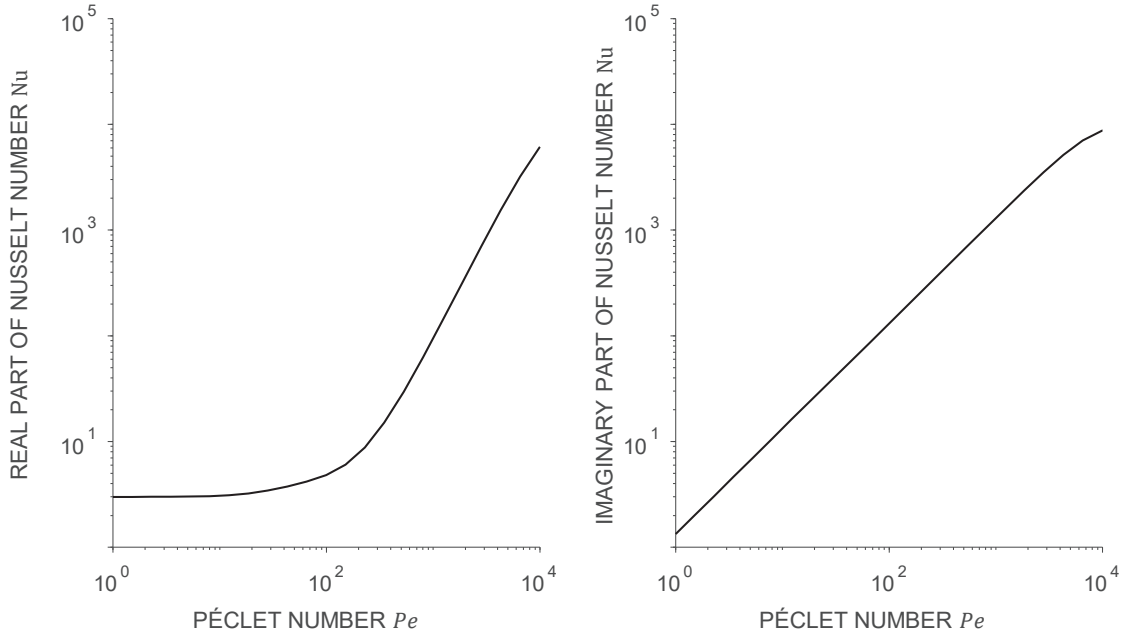

Figure 5: Resulting real and imaginary part of Nu for parameters of the tested accumulator

Figure 5 shows the results of the model for the parameters of the tested accumulators. Hence the model is able to cover the frequency-dependent rise of the real part of Nusselt number Nu' at a frequency of $Pe \sim 10^3$ and a continuous rise of the imaginary part of the Nusselt number Nu'', c.f. Figure 1. Size and ratio of the real and imaginary part of Nu contain information about the magnitude and the phasing behaviour of $\dot{q}$ and $T - T_\mathrm{a}$.

3 Validation

For the purpose of validating the model we performed measurements on commercial membrane accumulators.

3.1 Test Rig and Parameter

Figure 7 shows the tested commercial membrane accumulator. The test object is excited by a position-controlled cylinder in a servo hydraulic test rig and its pressure response is measured. The servo hydraulic test rig "test damper system 850" from MTS Systems is able to deflect various uniaxial devices dynamically, cf. Figure 6. Deflection, compression force and the resulting pressure were measured.

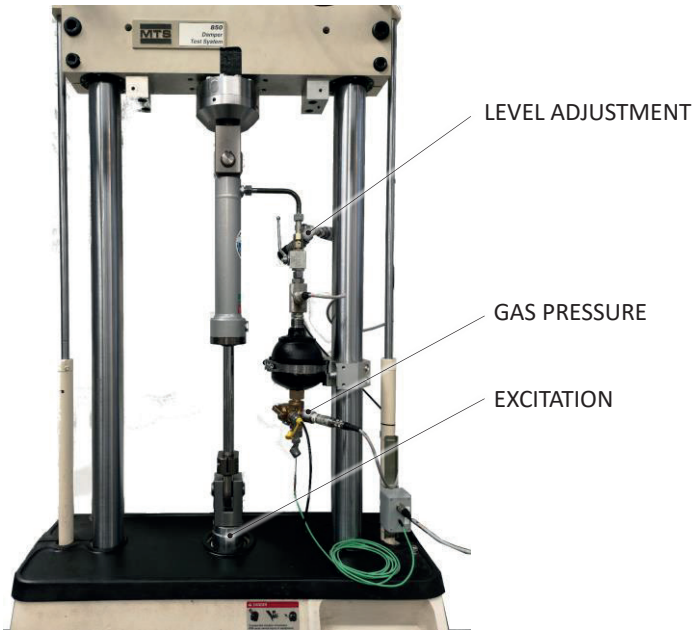

Figure 6: Test rig for dynamic characterisation of hydraulic accumulators [8]

Figure 7: Membrane accumulator for validation

The dynamic test rig for hydraulic accumulators shown in Figure 6 was first described in Rexer et al. [8]. Details can also be found in Hartig et al. [2] and Hartig [9]. In this case, the excitation is realized by means of a hydraulic cylinder integrated in the test rig. The accumulators are hydraulically connected to the cylinder. The volume is determined by the displacement-controlled excitation signal with the aid of the cylinder surface A_{cyl}. The accumulators are preloaded and hydraulically set to the desired load pressure by the level adjustment. Figure 7 shows an example of the investigated membrane accumulators. Table 1 contains all geometric and material parameters of the investigated accumulator needed for the model parameters.

The device is harmonically excited at amplitudes ranging from 4 ml to 8 ml and a frequency range of $f = 0.01 \ldots 20$ Hz. The accumulator is excited until it reaches a quasi-steady state and the hysteresis curve of the pressure response is closed. Then five cycles are measured and recorded. The last cycle is then analysed using first i) measurements of the pressure response of the hydraulic accumulators, cf. Figure 8. The measurement data are smoothed ii) since in step iii) numerical derivatives are calculated. In step iii) the constitutive equation for the gas and the momentary energy balance, cf. Eq. 2 and 3, are used to calculate heat flux $\dot{q} = \dot{Q}/A_{\mathrm{w}}$ and bulk temperature $\bar{T}$. Finally, iv) heat flux and temperature data are used to fit real part Nu' and imaginary part Nu'' of the complex Nusselt number.

parameter	hydraulic accumulator SBO500-0,1A6/112U-500AK
gas volume V_0 in m^3	$V_0 = 9.2 \cdot 10^{-5}$
effective heat transfer area A_w in m^2	$8.8 \cdot 10^{-3}$ [9]
cross sectional area cylinder A_cyl in m^2	$1.9635 \cdot 10^{-3}$
specific surface area s in m^{-1}	95.6
ambient temperature T_a in K	303
wall material	ST37 // 1.0315
average wall thickness l_wall in mm	10
density wall ϱ_wall in $\mathrm{kg/m}^3$	7.85 [10]
specific heat capacity wall c_wall in kJ/kgK	0.43 [10]
thermal conductivity wall λ_wall in W/mK	57 [10]
thermal conductivity gas λ in W/mK	0.028 @ 50 bar [11]

Table 1: Geometric and material parameters of the tested accumulator

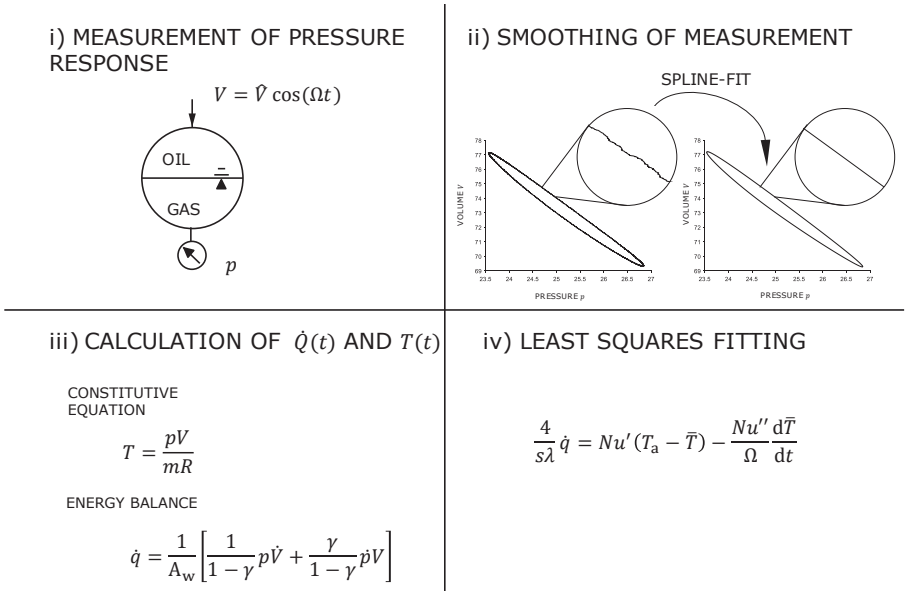

Figure 8: Methodology for measuring and fitting heat flux and bulk temperature in hydraulic accumulators [2]. The spline-fitting routine is based on least squares spline modelling [12].

3.2 Model and Measurement Results

In the analysis we use a previously developed regression method for obtaining real and imaginary parts of the complex Nusselt number [2]. Using the model introduced in Section 2, a master curve for the Nusselt number is obtained that describes the heat transfer behaviour for the accumulator.

Figure 6 shows the real and the imaginary part of the Nusselt number of the analysed measurements as well as the model results. The proportional constant is found by a least square fit and set to $K = 1.22$. All other resistances and capacities were calculated using the parameter of Table 1.

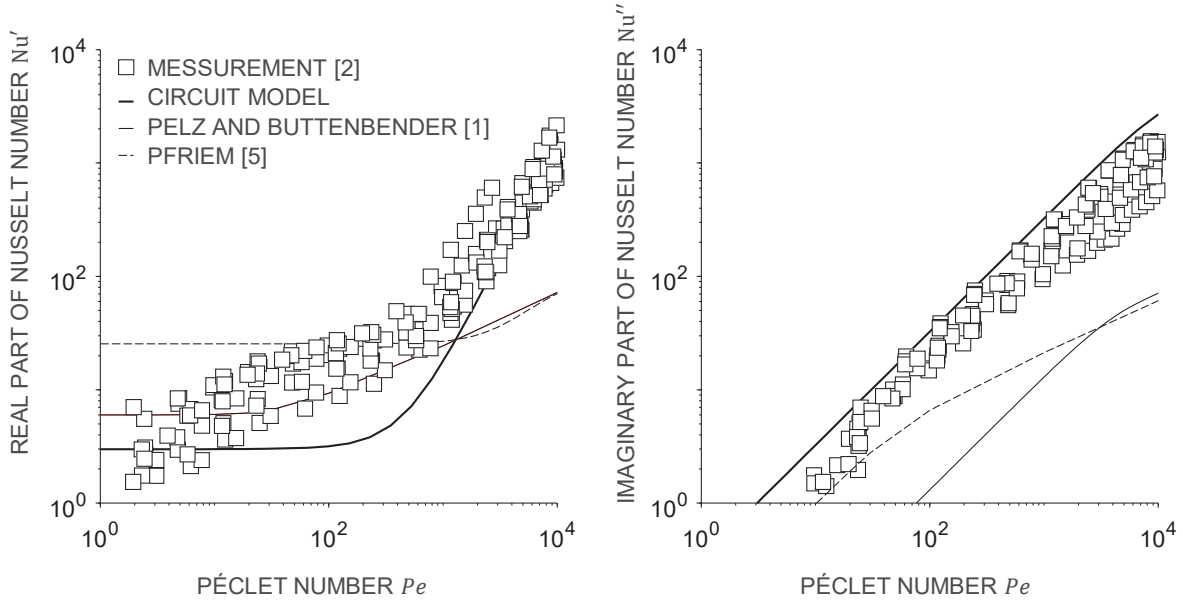

Figure 9:Model and measurement data given by Hartig et al. [2] and comparison to models by Pelz and Buttenbender [1] and Pfriem [5]. The proportionality constant of the boundary layer's capacitance K is set to 1.22 by least square fitting.

Comparing measurement data and circuit model results both parts of the complex Nusselt number Nu can be predicted by the model in a reasonable way. Especially the imaginary part of the Nusselt number seems to be covered by the model quite well. Former results of Buttenbender and Pelz [1] as well as Pfriem [5] lead to the conclusion that the main characteristics of the curves can be captured, but parameter optimisation is necessary.

4 Summary and Conclusion

A lumped-element model for dynamic heat transfer calculations in dynamically excited gas volumes has been presented. The proposed circuit model for heat transfer in reciprocating devices has been successfully applied to a first set of experimental data. The thickness of the thermal boundary layers is frequency-dependent, $\delta \propto Pe^{-0.5}$. The capacitive effect of forming thermal boundary layers changes the overall impedance of the unsteady heat transfer problem which in turn leads to phase-shifting behaviour of heat-flux $\dot{q}$ and ΔT. Thermal boundary layer formation is accompanied by an altered mass density distribution close to the wall.

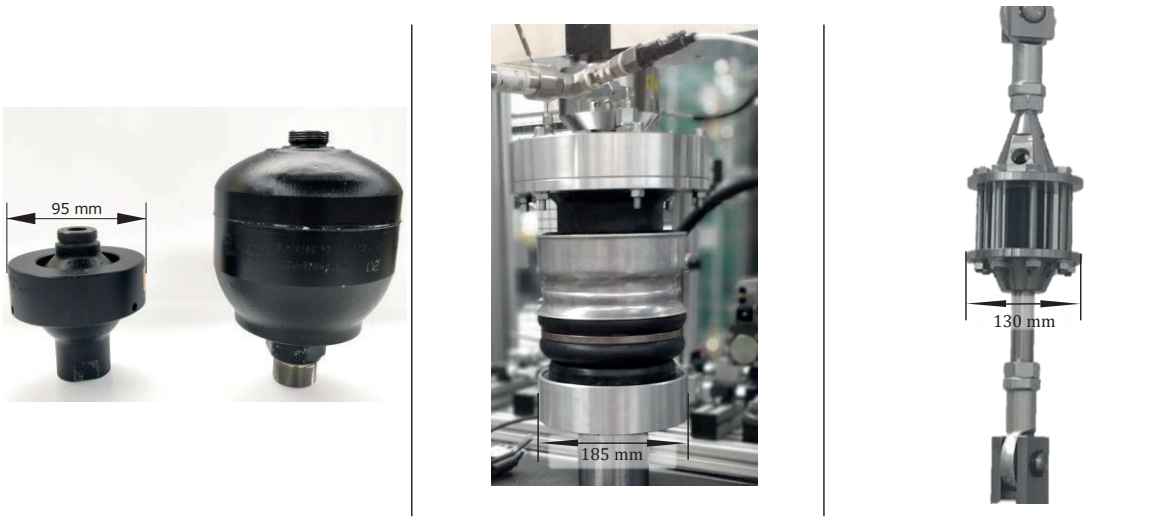

a) hydraulic accumulator *b) air spring* *c) pneumatic cylinder*

Figure 10: Three possible reciprocating devices with an enclosed gas for further investigation and model validation

Further research will be done on understanding the physical processes resulting in the boundary layers, focusing the nonlinearity of the resulting capacity $C_{\mathrm{bound}}(\Omega)$. The thermal and mechanical transfer behaviour of various, related devices, cf. Figure 10, will be investigated in order to understand the interaction between heat flux and excitation. Thus, the existing model will be adapted to be able to describe the transfer behaviour of these devices in their respective technical application.

5 Acknowledgements

Funded by the Deutsche Forschungsgemeinschaft (DFG, German Research Foundation) – project number 57157498 – SFB805.

Nomenclature

Variable	*Description*	*Unit*
a	Speed of Sound	m/s
A	Area	m²
A_{wall}	Wall Surface Area	m²
A_{cyl}	Cylinder Area	m²
c_{p}	Specific Heat Capacity	J/kgK
c_{wall}	Specific Heat Capacity of the Wall	J/kgK
C	Thermal Capacity	m²K/J
f	Excitation Frequency	Hz
Gr	Grashof Number	-
He	Helmholtz Number	-
l_{wall}	Average Wall Thickness	m

p	Pressure	bar(a)
Pe	Péclet Number	-
$\dot{q}$	Surface Specific Heat Flux	W/m²
$\dot{Q}$	Heat Flow	W
$\mathcal{R}$	Specific Gas Constant	J/kgK
R	Thermal Resistance	Km²/W
Re	Reynolds Number	-
s	Specific Surface Area	1/m
t	Time	s
T	Temperature	K
T_a	Ambient Temperature	K
V	Volume	m³
y	Cylinder Coordinate	m
$\tilde{y}$	Dimensionless Cylinder Coordinate	-
Z	Thermal Impedance	Km²/W
$\mathcal{Z}$	Compressibility Factor	-
γ	Isentropic Exponent	-
δ	Boundary Layer Thickness	-
λ	Thermal Conductivity	W/mK
λ_wall	Thermal Conductivity of the Wall Material	W/mK
ϱ	Density	kg/m³
ϱ_wall	Density of the Wall Material	kg/m³
Ω	Angular Frequency	1/s

References

[1] Pelz, P. F., Buttenbender, J., *The dynamic stiffness of an air-spring*, In: International Conference on Noise and Vibration Engineering, Katholieke Universiteit Leuven - Departement Werktuigkunde, pp. 1727-1736, 2004.

[2] Hartig, J., Depp, B., Rexer, M., Pelz, P. F., *Effects of Unsteady Heat Transfer on Behaviour of Commercial Hydro-Pneumatic Accumulators*, Preprint, Available from *https://arxiv.org/pdf/2012.06526*, 2020.

[3] Kornhauser, A. A., Smith, J. L., *Application of a Complex Nusselt Number to Heat Transfer During Compression and Expansion*, Journal of Heat Transfer(3), 536-542, 1994.

[4] Kornhauser, A. A., Smith, J. L., *The Effects of Heat Transfer on Gas Spring Performance*, Journal of Energy Resources Technology(1), 70-75, 1993.

[5] Pfriem, H., *Der periodische Wärmeübergang bei kleinen Druckschwankungen*, Forschung auf dem Gebiet des Ingenieurwesens(2), 67-75, 1940.

[6] Watson, G. M., Stevens, A. B., Evans, R. B., Hodges, D., *Compressibility Factors of Nitrogen-Propane Mixtures in the Gas Phase*, Ind. Eng. Chem.(2), 362-364, 1954.

[7] Schlichting, H., Gersten, K., *Grenzschicht-Theorie*, Springer, Berlin, Heidelberg, 2006.

[8] Rexer, M., Kloft, P., Bauer, F., Hartig, J., Pelz, P. F., *Foam accumulators: packaging and weight reduction for mobile applications*, In: Volume 1 - Symposium, 12th International Fluid Power Conference, Technische Universität Dresden (Ed.). Dresden, pp. 181-188, 2020.

[9] Hartig, J., *Hydrospeicher mit Adsorbentien*, Forschungsberichte zur Fluidsystemtechnik, Shaker, Aachen, 2021.

[10] VDI-Gesellschaft Verfahrenstechnik und Chemieingenieurwesen (Ed.), *VDI-Wärmeatlas*, Springer Vieweg, Berlin, 2013.

[11] Linstrom, P., W.G. Mallard (Eds.), *NIST Chemistry WebBook, NIST Standard Reference Database 69*, National Institute of Standards and Technology, Gaithersburg MD, 1997.

[12] D'Errico, J., *SLM - Shape Language Modeling MATLAB Central File Exchange. Retrieved January 7, 2022.*, MATLAB Central File Exchange, 2022.